Optics and Laser Technology 109 (2019) 178–185

Contents lists available at ScienceDirect

Optics and Laser Technology

journal homepage: www.elsevier.com/locate/optlastec

Full length article

Detecting beam offsets in laser welding of closed-square-butt joints by wavelet analysis of an optical process signal

Arianna Elefante[a], Morgan Nilsen[b,*], Fredrik Sikström[b], Anna-Karin Christiansson[b], Tommaso Maggipinto[a], Antonio Ancona[b,c]

[a] University of Bari, Physics Department, Via Amendola 173, 70126 Bari, Italy
[b] University West, Department of Engineering Sciences, 461 80 Trollhättan, Sweden
[c] IFN-CNR Institute for Photonics and Nanotechnologies, Physics Department, Via Amendola 173, 70126 Bari, Italy

HIGHLIGHTS

- Narrow laser welded butt joints are monitored by a photodiode system.
- The photodiode signal is analyzed using continuous wavelet transform.
- The system is evaluated by both continuous wave and pulsed mode laser beam welding.
- The wavelet transform signal detects fast beam deviations from the joint.

ARTICLE INFO

Keywords:
Laser beam welding
Joint tracking
Butt joints
Photodiode
Wavelet analysis

ABSTRACT

Robotized laser beam welding of closed-square-butt joints is sensitive to the positioning of the laser beam with respect to the joint since even a small offset may result in a detrimental lack of sidewall fusion. An evaluation of a system using a photodiode aligned coaxial to the processing laser beam confirms the ability to detect variations of the process conditions, such as when there is an evolution of an offset between the laser beam and the joint. Welding with different robot trajectories and with the processing laser operating in both continuous and pulsed mode provided data for this evaluation. The detection method uses wavelet analysis of the photodetector signal that carries information of the process condition revealed by the plasma plume optical emissions during welding. This experimental data have been evaluated offline. The results show the potential of this detection method that is clearly beneficial for the development of a system for welding joint tracking.

1. Introduction

Robotized laser beam welding (LBW) of closed-square-butt joints enables efficient joining of complex structures giving high quality seams with narrow widths [1]. This is feasible since the laser beam can be focused into a small spot on the work piece. However, due to the narrow fusion zone, the process requires accurate joint preparation, fixturing and robot motion. Besides from this, laser induced distortions may occur during welding and these factors can lead to welding with an offset between the laser beam spot and the actual joint position. Welding with an offset from the joint position may cause lack of sidewall fusion within the seam, as shown in the weld cross section in Fig. 1. This is a critical defect giving a weak seam and it is hard to detect even when using non-destructive test methods. This defect is neither visible on the top nor on the root side of the seam, so non-destructive test methods, such as ultrasonic testing, could fail due to the orientation of the thin defect.

Joint tracking systems are used to avoid this problem and there are several commercial systems available, examples can be found in [2–4]. They use a sensor, usually a camera together with one or several laser lines utilizing the triangulation principle, to measure the joint position and control the laser tool position. However, with machined parts and high fit-up tolerances of the work piece, these systems have low detection probability when the joint gap width and misalignment are close to zero. Scratches may also be present near the joint that can be misinterpreted as the actual joint and mislead the tracking system. In addition, there might be tack welds that covers the joint so that optical detection in that area is impossible.

Several researchers have addressed the issue of joint tracking of zero gap (< 0.1 mm) square-butt joints. The basic concepts for joint tracking

* Corresponding author.
E-mail address: morgan.nilsen@hv.se (M. Nilsen).

https://doi.org/10.1016/j.optlastec.2018.08.006
Received 13 February 2018; Received in revised form 30 July 2018; Accepted 2 August 2018

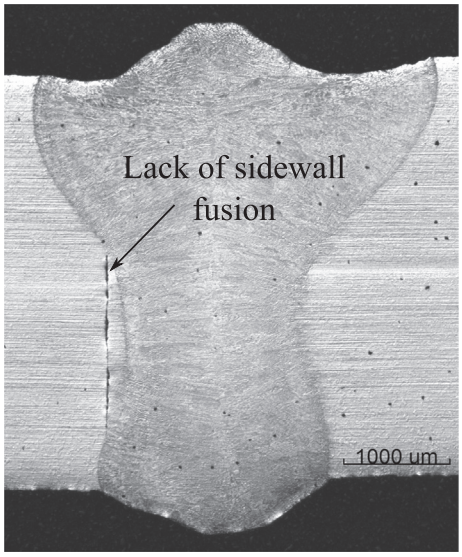

Fig. 1. Cross section of closed-square-butt seam when welded with the laser beam at a 1 mm offset from the joint.

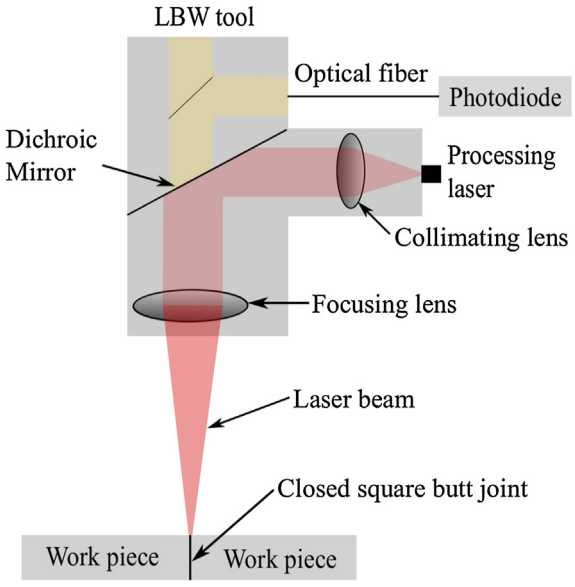

Fig. 2. The LBW tool and its integration of the photodiode.

and specific problems related to this are described in [5], where a multifunctional joint tracking sensor is presented, based on a CMOS camera and low power laser illumination, used for joint tracking and for measuring the displacement between the LBW tool and the work piece. A method to track narrow joints using a CCD camera and a vision algorithm is described in [6], and promising results are shown for an arc welding application. In [7], a texture based algorithm is suggested, where the difference in surface texture of the two work pieces is used to find the joint position from images obtained by a CMOS camera during LBW. In [8], narrow weld joint gaps are tracked using a combination of 2D feature extraction and 3D laser triangulation. An infrared camera, placed in an off-axis configuration, is used in [9] to capture images of the melt pool, and from that information track the joint position during LBW. In [10], a magneto-optical sensor is used to track narrow gaps (< 0.1 mm) during LBW. Although these systems show promising results, this paper investigates the possibility to use a relatively cheap photodiode, which is easy to integrate into an industrial LBW system, for the same purpose.

Many researchers have addressed the issue of finding correlations between the LBW process behavior and the signals from photodiodes. Compared to other optical sensors, photodiodes are inexpensive, fast and easy to integrate into the LBW system. Several commercial monitoring systems are available, using photodiode signals to find correlations to the LBW process behavior, see e.g. [2,11–15]. A feedback control system for full-penetration welding using two photodiodes is presented in [16]. A closed loop system to maintain an even seam is presented in [17], a photodiode is here placed on the root side of the work piece during CO_2 LBW. In [18], a technique is developed for monitoring focus and power variations by chromatic filtering. The relationship between welding defects and a photodiode signal is also investigated in [19], and a mathematical model for numerical simulation is developed. Often, in photodiode-based monitoring and control systems, an upper and a lower threshold are set, and deviations in the LBW process are indicated if the signal is outside these thresholds. The thresholds need calibration for each situation in order not to give false detections and at the same time detect real deviations, which might be a difficult task. It is clear that the signals from the photodiodes hold valuable information about the LBW process, but the interpretation of this information needs to be conducted not just by looking at the level of the raw intensity data from the sensor [12].

More complex signal processing is required to extract the information related to the LBW process quality from the raw photodiode signals. Fuzzy multi-feature pattern recognition algorithms [20] or frequency analyses of the signals through Fast or Short-Time Fourier Transform algorithms have been often used in the past, also for application to LBW process monitoring [21]. However, Fourier methods are not always a good solution to analyze signals that undergo sudden changes, fluctuations or discontinuities, as is the case of LBW. In addition, such methods do not yield a time-resolved analysis of the signals, which is essential to develop in-situ and real-time control systems.

The wavelet transform (WT) provides the frequency analysis of a signal in the time domain, thus enabling a time-frequency representation. There are two different kinds of wavelet transform: continuous and discrete [22,23].

A wavelet is a waveform highly localized in time. In a simple way, Continuous Wavelet Analysis (CWA) can be defined as the convolution of the original signal with a continuously scaled and shifted version of the wavelet function. While the Fourier Transform decomposes a signal into infinite length sines and cosines, effectively losing all time-localization information, the CWA by means of wavelets as basis functions allow for time-frequency analysis. The numerical output of CWA consists of the so-called wavelet coefficients. Wavelet coefficients are evaluated at every possible scale and wavelet functions need not to be orthogonal basis functions.

If only a subset of scales and position is chosen (usually dyadic scales and positions) and if basis functions are required to be orthogonal, then we obtain the so-called Discrete Wavelet Analysis (DWA).

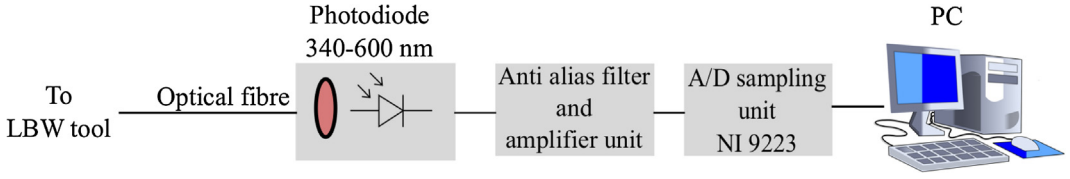

Fig. 3. Principle of the photodiode system.

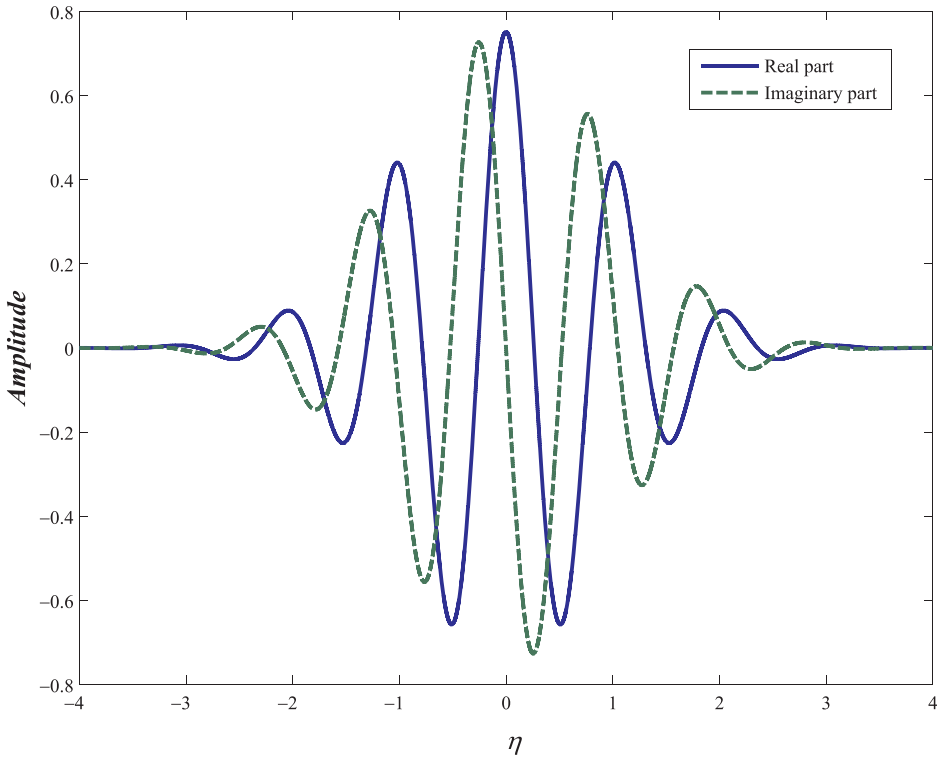

Fig. 4. Morlet wavelet function.

DWA is more suited for the so-called multiresolution analysis and to highlight trends in signals. On the other side, the advantage of CWA relies on smooth variation of local frequency and scales and on an easier detection of discontinuities. Therefore, it is an invaluable tool for the analysis of non-stationary time series.

In the very few studies found in literature concerning the wavelet time-frequency analysis of signals generated during LBW, the DWA algorithm was used. In [24,25] airborne acoustic signals were analyzed and, based on the DWA results, tools were constructed as an artificial neural network of the signal intensity moving average to diagnose welding defects. However, the noisy environment of welding workshops hinders real industrial applications using acoustic sensors. In [26] the spectral emissions from the plasma plume in a laser process were analyzed by using DWA. In this way the formation of pores could be successfully detected and it is also indicated that this method could be used to detect other welding errors. In [27] the electrode pressure signal in resistance spot welding were measured and analyzed by DWA. Results show that splashing defects could be detected by using the presented method.

In [28], the plasma plume was monitored during CO_2 LBW using a single silicon photodiode. The acquired signal was analyzed using the DWT variations caused by changes of incident laser power or shielding gas flow. A wavelet packet decomposition and principal component analysis of photodiode and spectrometer signals acquired during LBW processes was applied in [29] to estimate and classify the welding status. A data-driven model was established by applying multivariate statistics and machine learning methods, and, subsequently, validated through a comparison with welding images captured by laboratory visual sensors. In [30], the DWT analysis of the signals recorded by three different photodiodes allowed to detect transitions between deep keyhole and conduction welding modes originated by abrupt changes of the laser power. Although showing some promising results, the welding tests were only performed in cases affected by macroscopic defects artificially produced by sudden and big variations of the process conditions, which are unlikely in a real production scenario.

The aim of this contribution is to evaluate the potential of the CWA algorithm applied to the plasma plume light intensity signal acquired by a cheap photodiode during LBW. This detector, placed coaxially with the laser beam, is able to detect slow variations of the process conditions, like in the case of the evolution of an offset between the laser beam spot and the joint in robotized LBW of closed-square-butt joints. This method has been applied and evaluated with different robot trajectories, i.e. following the joint without any offset, going out of the joint quickly, with a step-like movement, or slowly, with a ramp like movement. The laser was operated both in continuous wave (c.w.) and in pulsed mode to see if the frequency content of the signal was influenced by any time variation of the laser source output power. Finally, a comparison with bead-on-plate, tests performed with identical robot paths and LBW process conditions have been carried out.

2. Experimental setup and procedure

2.1. Laser system setup and weld material

LBW tool manipulation was conducted using an industrial robot, ABB IRB4400. The position of the tool center point was continuously recorded synchronized with the photodiode data in order to correlate signal changes to the laser spot position on the work piece. The laser source used was a 1070 nm wavelength fiber laser, IPG Ytterbium Fiber Laser (YLR-6000-S, 6 kW), and the LBW tool was from Permanova Lasersystem AB. The setup using a 160 mm focal length collimator, a 300 mm focal length focusing lens and a 600 μm optical fiber gave a laser beam spot diameter of 1.12 mm and a Rayleigh length of 13.7 mm. The reason for choosing this relatively large laser spot diameter was due to that welding was performed with an industrial robot with limited path accuracy. A larger spot diameter gives in this case a more robust process since a wider seam is achieved. The laser beam spot was focused on the work piece surface and the laser power was 2750 W for c.w. laser and 3000 W (high level)/1300 W (low level) for pulsed laser experiments resulting in keyhole welding in both cases. The robot speed was 9.6 mm/s. The laser power and robot speed was experimentally derived in order to produce a visibly good looking weld seam.

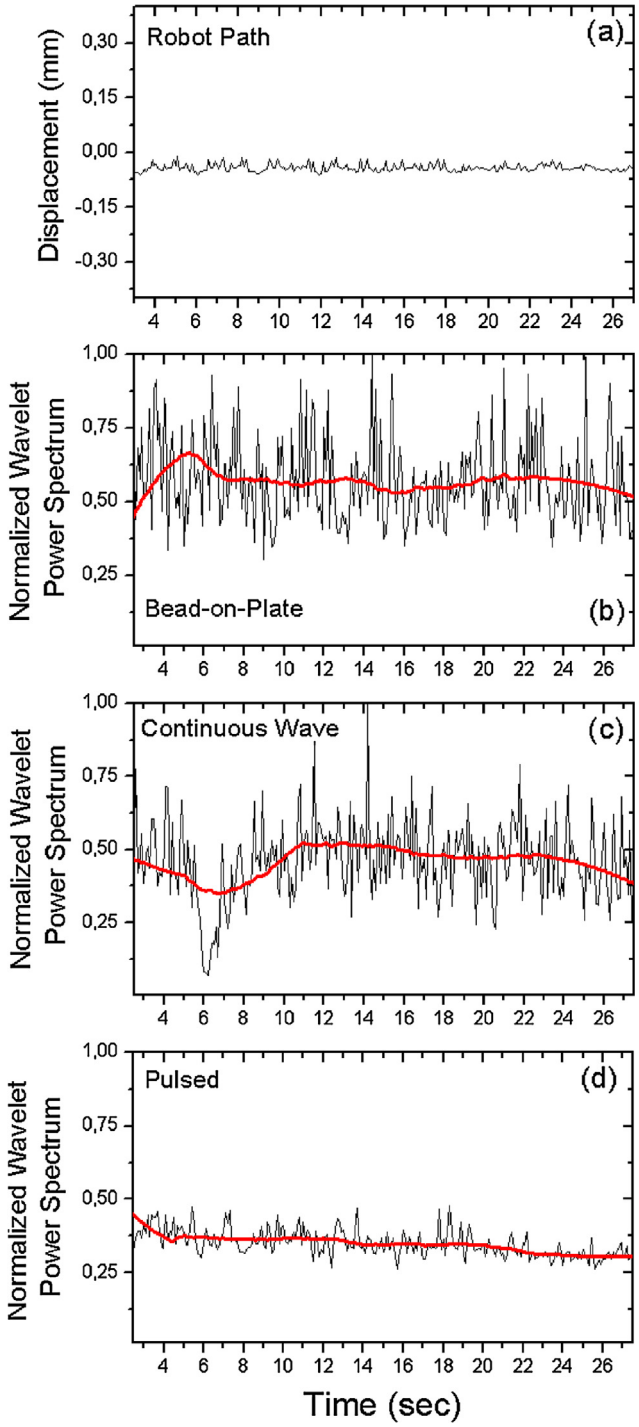

Fig. 5. Results from a "Reference" weld in the following order: (a) measured robot displacement; (b) NWPS signal (black-thin) and smoothed signal (red-thick) in case of bead-on-plate, (c) c.w. laser operation, and (d) pulsed mode laser operation. (For interpretation of the references to colour in this figure legend, the reader is referred to the web version of this article.)

Welding was conducted without filler material, and the material used was 4 mm thick stainless steel (316) metal plates in a closed-square-butt joint configuration with technical zero gap. The plates were manually tack welded (approximately 50 mm between each tack weld) and clamped in a fixture to restrict heat induced distortions and changes in gap width during welding. Argon was supplied as shielding gas on the top side with a flow rate of 32 l/min through a 10 mm in diameter tube, and also on the root side through a gas channel integrated in the fixture. Argon was also supplied in front of the focusing lens of the LBW tool to protect it against spatter from the vapor plume.

2.2. Photodiode monitoring system

A monitoring system using a photodiode with a specific spectral range has been developed to monitor the plasma plume optical emission from the LBW process. The photodiode is coaxially integrated into the LBW tool as shown in Fig. 2.

A fiber coupled silicon photo detector, Thorlabs PDA100A-EC, sensitive to wavelengths between 340 and 1100 nm is used for monitoring. The spectral range is limited to a range between 340 and 600 nm by an optical filter. At this spectral range, it is able to detect high temperatures representing the vapor plume above keyhole. Fig. 3 shows an illustration of the photodiode system.

The photo detector is connected to a unit containing an anti-aliasing filter designed as a 4th order active low pass filter with a cut-off frequency at 120 kHz (−3 dB) and a voltage amplifier. The filter prevents aliasing, and the amplifier amplifies the relatively low output signals from the photodiodes, with approximately 10 times amplification factor, to get a signal level between 0 and 10 V. The output signal from the filter/amplifier unit is connected to an analog input module with a 10 V input range and 16-bit resolution. A LabVIEW application, running on a PC using Windows, saves the measured intensity data in a log file synchronized with the robot position data. This data is later analyzed off-line using Matlab.

2.3. Welding procedure

Three different test cases have been conducted to evaluate the performance of the monitoring system. Beam movement was conducted by programming the welding path of the industrial robot holding the laser beam welding tool. Each of the test cases were repeated three times, all using both c.w. and pulsed laser:

1. "Reference": welding in a straight joint with a minimal offset between the joint and the focused laser beam spot.
2. "Steps-out-of-the-joint": Welding started with no offset between the joint and the laser beam spot and was then moved sideways away and back to the joint. Step size was 1.2 mm and the duration at each position was 25 mm. This was repeated four times for each weld. This test was conducted in order to evaluate the monitoring system's ability to handle quick deviations with respect to the joint position.
3. "Ramp-out-of-the joint": Welding started with no offset between the joint and the laser beam spot. After 80 mm, the beam spot was linearly moved away from the joint in a ramp, during 70 mm movement, until it was 5 mm away from the joint, when it was moved back linearly into the joint in an opposite motion. This test was conducted in order to evaluate the monitoring system's ability to handle slow deviations with respect to the joint position.

3. Wavelets

As it is well known, the Fourier Transform can be seen as a mapping of a stationary signal from the time (or space) domain to the frequency domain; this task is accomplished through sine and cosine wave basis. As a result, if a signal changes at a specific time, its transform changes everywhere and the sole inspection of the transformed signal cannot give any information about the time localization of the variation. This disadvantage can be overcome in first instance by performing the Fourier transform on a sliding window of a certain length, although the method proves to be inaccurate and inefficient from the point of view of frequency localization, since several window lengths should be used.

The continuous wavelet transform (CWT) [31] offers an efficient way of addressing the analysis of non-stationary signals containing

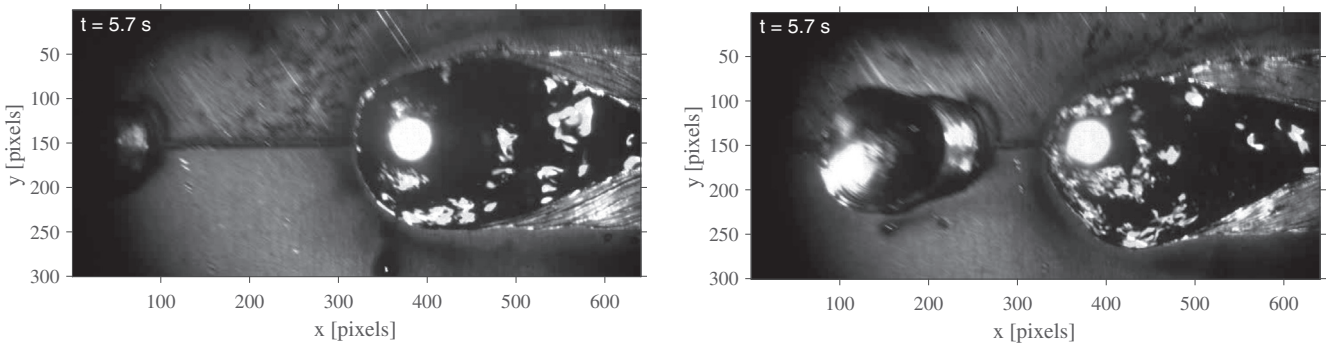

Fig. 6. Snapshot of the LBW pool acquired by a coaxial camera (a) just before and (b) during the process disturbance detected at the time $t = 6$ s of the "Reference" weld test case performed operating the laser in c.w. (see Fig. 5c).

power at different frequencies and at different times. It is based on a signal that is convoluted with a scaled and translated version of a locally confined function, called wavelet mother function. The mother function has to be localized in time and space and depends on two parameters, n for translation and s for dilation. The parameter n shifts the wavelet so that local information around time $t = n$ is contained in the transformed function. The parameter s controls the window size in which the signal analysis must be performed. In this way, the wavelet function acts as a varying probe for the initial time signal.

Several features should be considered when choosing a wavelet mother function. General considerations are reported in [32].

One of the most common non-orthogonal wavelet function is the so called Morlet Function which is composed of a complex exponential multiplied by a Gaussian function and represents the best trade-off between time and frequency resolution [31].

In this work, we have adopted the Morlet function, represented in Fig. 4, as wavelet mother function with the mathematical expression

$$\psi_0(\eta) = \pi^{-1/4} e^{-i\omega_0\eta} e^{-\eta^2/2}$$

where η is a non-dimensional time parameter and ω_0 is the non-dimensional frequency parameter, which was set to 6 to satisfy the admissibility condition for the function to have zero mean and to be localized in both time and frequency space [31]. The relation of those parameters with the physical time and physical frequency can be derived from the sampling time of the original time series and by exploiting the relation existing between ω_0 and the corresponding Fourier frequency [32].

By varying the parameters s and n, different time scaled and translated versions of the mother wavelet have been constructed in order to analyze the signal at different times and frequencies:

$$\psi_{n,s}(\eta) = \left(\frac{\delta t}{s}\right)^{1/2} \psi_0\left[\frac{(\eta - n)\delta t}{s}\right]$$

where δt is the physical sampling rate, which for our photodiode is $\delta t = 10^{-6}$ sec and s is the set of scaled used defined as follows:

$$s_j = s_0 2^{j(\delta j)}, \quad j = 0, 1, \cdots, J$$

$$J = (\delta j)^{-1} \log_2(N\delta t / s_0)$$

where N is the number of data points in the acquired time series and s_0 is the smallest resolvable scale. The latter is usually chosen so that the equivalent Fourier period is approximately $2\delta t$. When dealing with Morlet mother function it is possible to set s_0 exactly equal to $2\delta t$. The maximum frequency that can be analyzed owing to the Nyquist theorem in our case is approximately 48.5 kHz. The parameter J defines the largest scale and corresponds to the limit case where the length of the wavelet and of the function to analyze are the same. It determines the smallest frequency analyzed, set to 1.5 Hz. Finally, δj represents the separation between subsequent scales, which has been set to 0.04 to have adequate frequency resolution.

The wavelet analysis has been carried out by employing the Torrence and Compo Open source code [32]. In particular, after calculating the CWT, the Wavelet Power Spectrum has been computed as the absolute square of the CWT. Afterwards, the Normalized Wavelet Power Spectrum (NWPS) was estimated by integrating the spectrum over the desired sliding time window and dividing it by the number of points contained in that window.

Initially, a broad frequency band, from 1.5 Hz to 48.5 KHz, was examined. This range has been divided into sub-bands to better identify the signal's frequencies whose time variation was more sensitive to change of the process conditions.

4. Results and discussion

The acquired photodiode signals have been analyzed using the CWT algorithm described in Section 3. The raw data relating to the experiments performed with the laser operating in pulsed mode were preprocessed using a Comb filter in order to eliminate the frequency components corresponding to the laser repetition rate and its entire higher harmonics.

The preliminary evaluation of the wavelet power spectra revealed that, among all the bands examined, the range between 410 Hz and 7.1 kHz contained most of the spectral signal component frequencies. This result is in well agreement with previous works, which found that the dominant frequency band of high-power LBW plasma spectral emission oscillations, under stable and sound process conditions, lies in the range between 200 Hz and 15 kHz [28].

For this reason, the following CWT results refer to the frequency range from 410 Hz to 7.1 kHz. In particular, for each welding experiment the NWPS signals are presented, where each point of the signal has been calculated over a sliding window of 100 ms time duration.

Fig. 5 shows representative results from sound welds, i.e. "Reference test", where laser beam spot was almost perfectly aligned with the gap along the entire joint. In the top graph (Fig. 5a), the robot path is depicted with the time evolution of the displacement of the center of the laser beam from the joint. The three following graphs show the NWPS signals, respectively, for a straight bead-on-plate (Fig. 5b), and two "Reference" in-joint butt welds performed by operating the laser in c.w. (Fig. 5c) and pulsed mode (Fig. 5d). It can be noticed that, except for a sudden and short time drop located at around $t = 6$ s after the start of the c.w. laser weld, in most cases the NWPS signal oscillates around an average value which stays almost constant along the entire welding joint under examination. This is even better highlighted by the smoothed signal (thick-red line) calculated by applying to the original NWPS a Savitzky-Golay filter [33] with a sliding window of 110 consecutive points.

As regards the localized drop of the signal noticed during the c.w. laser weld, a parallel investigation based on the acquisition of the weld pool images using a coaxial high-speed camera synchronized with a LED illumination system [34] revealed an evident process instability at

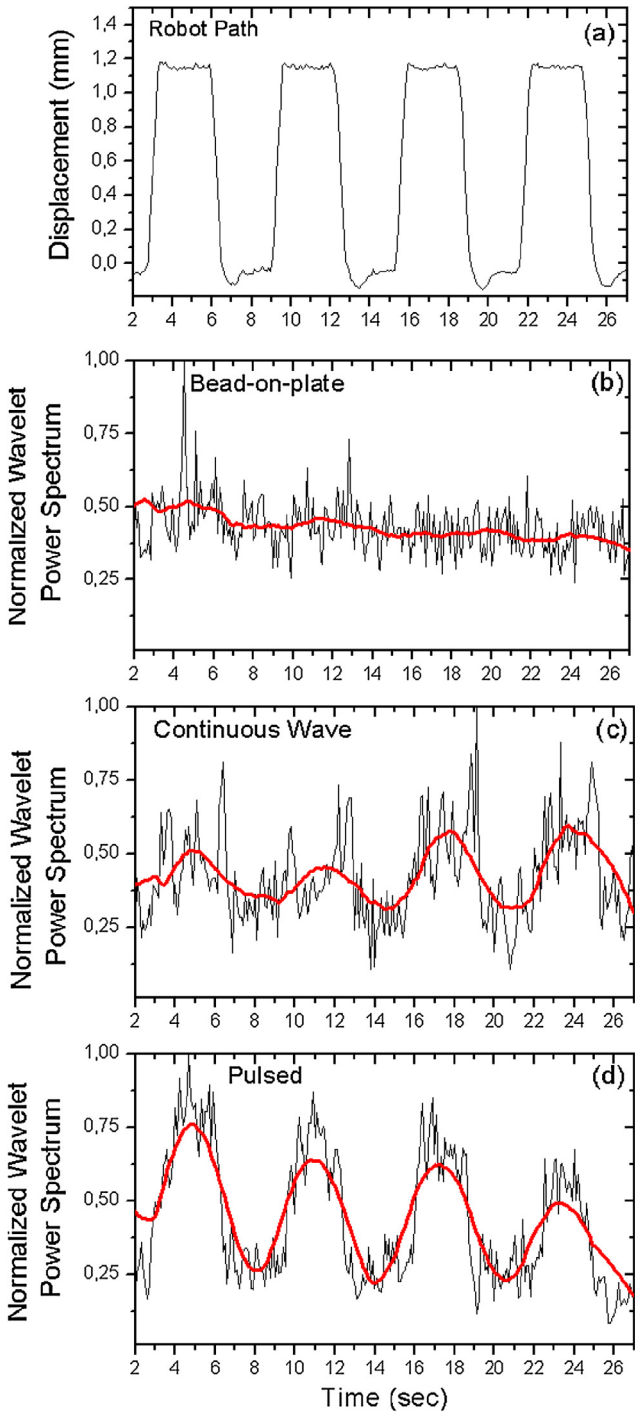

Fig. 7. Results from a "Steps-out-of-the-joint" weld in the following order: (a) robot displacement; (b) NWPS signal (black-thin) and smoothed signal (red-thick) in case of bead-on-plate, (c) c.w. laser operation, and (d) pulsed mode laser operation. (For interpretation of the references to colour in this figure legend, the reader is referred to the web version of this article.)

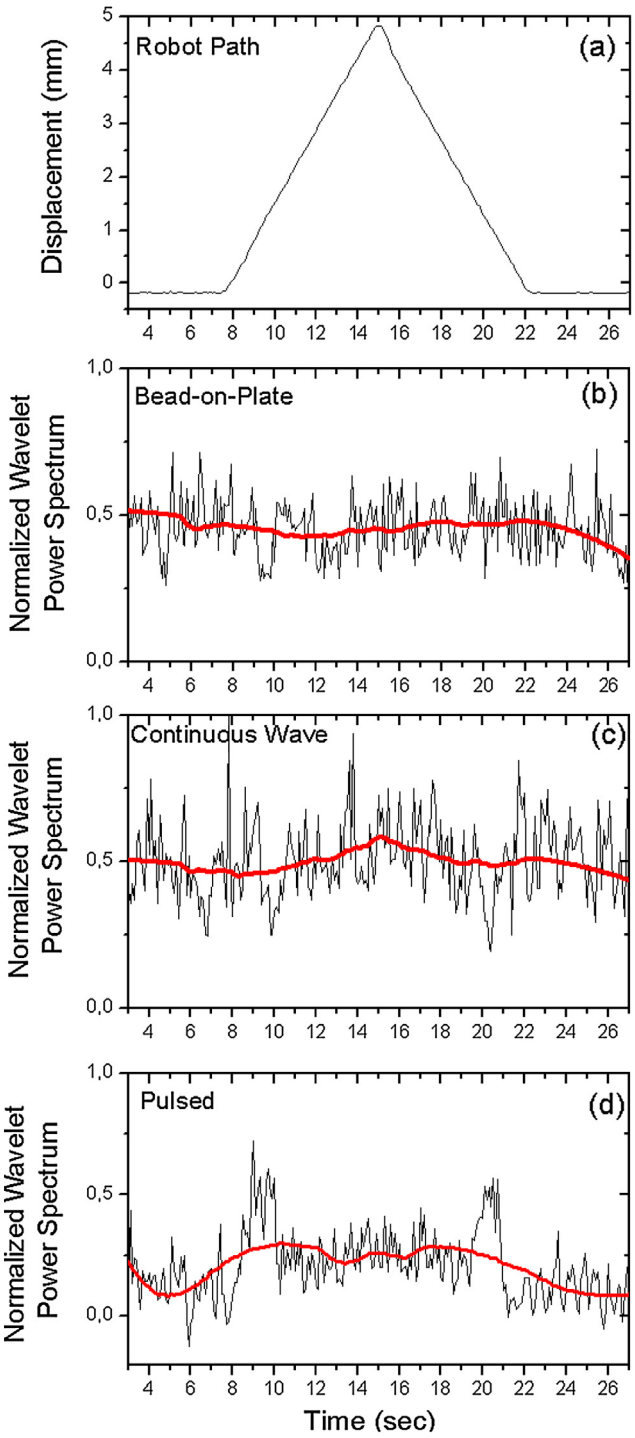

Fig. 8. Results from a "Ramp-out-of-the-joint" weld in the following order: (a) robot displacement; (b) NWPS signal (black-thin) and smoothed signal (red-thick) in case of bead-on-plate, (c) c.w. laser operation, and (d) pulsed mode laser operation. (For interpretation of the references to colour in this figure legend, the reader is referred to the web version of this article.)

the same instant. Fig. 6 shows two images acquired slightly before and during the process instability occurred at $t = 6$ s, respectively. While in the first frame the weld pool looks symmetric with respect to the laser beam, which is perfectly aligned with the joint, in the second frame, although the beam is still aligned with the joint, the weld pool is largely asymmetric thus revealing that a disturbance of the process occurred, probably leading to turbulences in the melt pool causing a weld flaw. Afterwards, for $t > 7$ s the melt pool returned to its original symmetric shape and the smoothed NWPS signal to its steady average value.

Fig. 7 shows results obtained for "Step-out-of-the-joint" welds. As it can be seen from Fig. 7a, the maximum lateral displacement of the laser beam from the joint gap is 1.2 mm, which is slightly bigger than the beam spot size, thus creating the conditions for lack of sidewall fusion. Here, while the NWPS signal referred to the bead-on-plate test do not display any sudden change when the laser beam is deviated from its straight path (Fig. 7b), in case of real welds evident variation of the wavelet power spectrum are noticed when the beam exits from the joint

for both laser operating modes (Fig. 7c and d). Again, the change of the NWPS is clearer by applying a Savitzky-Golay filter. This trend of the NWPS signal is verified to be reproducible and consistent every time a beam offset occurs within the same weld. Anyhow, the frequency power spectrum variation is more pronounced in case of pulsed LBW compared to c.w., as if the modulation of the laser power enhances the change of the spectral signal frequency content upon variation of the process conditions.

Results for the "Ramp-out-of-the joint" welds are reported in Fig. 8. The NWPS signal computed during the bead-on-plate test, once again, does not reveal any noticeable change of its average value along the entire joint. At a first glance, the analogous signal calculated for the weld tests performed in c.w. laser mode does not show a trend that plasma is clearly correlated to the beam path. Only some localized and abrupt oscillations of the signal, like e.g. in the ranges $8\,s < t < 10\,s$ or $20\,s < t < 22\,s$, are noticed (see Fig. 8c). However, by applying the Savitzky-Golay filter, the smoothed signal exhibits a clear trend. The NWPS starts to increase when the beam exits from the joint, it reaches its maximum value at the time of the highest displacement and then decreases back to its original value at the time of re-alignment with the joint. Such trend is confirmed also for pulsed LBW with the only exception that, in this case, transient and huge increases of the NWPS are found at the time when the beam goes out and back into the joint (Fig. 8d). It is anyhow confirmed that the pulsed operating mode amplifies the increase of the wavelet power spectrum, in the examined frequency range, when a change of the process conditions occurs.

All the experimental results presented in this section indicate that the frequency components in the band from 410 Hz to 7.1 kHz of the photodiode signals related to the LBW plasma plume spectral emission are more intense when the laser beam spot is focused with an offset to the joint gap. It can be concluded that the CWA is an effective tool to detect such variations. This result is strictly related to the beam-to-joint gap offset and not to the beam path, since during analogous bead-on-plate tests no variations of the NWPS signal was observed. Finally, this change of the intensity of the frequency components in the investigated range is more pronounced in case of pulsed mode operation of the laser source compared to c.w.

Such results open new scenarios in detecting lack of sidewall fusion during LBW of closed-square-butt joints with cheap and fast detectors like photodiodes. In addition, if related to specific feature of the keyhole or weld pool, the detected variations of the plasma plume emission in the frequency range investigated could help to better understand and model the physical interactions of laser keyhole welding.

5. Conclusions

This work presents a novel system for beam offsets detection in LBW of closed-square-butt joints. The CWA performed off-line is central in the system using the signals acquired by a photodiode for detection.

Welding experiment with different robot trajectories and with the processing laser operating in both continuous and pulsed mode provided data for an evaluation of the system performance.

Results show that the system is capable of capturing the evolution of a beam offset from the joint in different relevant LBW scenarios.

A comparison with previous work utilizing a dual vision and spectroscopic sensing approach [34] shows that the proposed system performs better than the spectroscopic sensing approach in the "Ramp-out-of-the joint" case, which is promising.

Closed loop joint tracking systems requires sufficiently fast recursive algorithms that satisfy real-time considerations. The knowledge about the specific frequency range in the photodetector signal that indicates the evolution of a beam offset from the joint is of great importance when designing such real-time estimation and change detection algorithms. Knowledge of the specific frequency range would also be useful to further improve the current keyhole welding models in case it was shown that those frequencies are related to fluid flow and/or vaporization dynamics. Advanced and more reliable models would potentially allow estimation and control of LBW.

The results in this work is a basis for future efforts towards real-time estimation and change detection. The photodetector signal is potentially useful to support a machine vision based closed-loop joint tracking system in LBW of closed-square-butt joints by providing a go/no go information in cases where a machine vision system fails in detecting the joint position.

Acknowledgements

This work was supported by the People Programme (Marie Curie Actions) of the European Union's Seventh Framework Programme (FP7/2007-2013) under REA grant agreement no 608473 (MoRE program project "Hy-Las" – Hybrid sensing for understanding of laser welding technology for process control). Funding from the VINNOVA project VarGa (2016-03291) is also acknowledged.

References

[1] W.M. Steen, J. Mazumder, Laser Material Processing, Springer, London, London, 2010.
[2] Precitec, http://www.precitec.de/en/ (accessed February 13, 2018).
[3] Scansonic, http://www.scansonic.de/en (accessed February 13, 2018).
[4] Permanova, http://permanova.se/ (accessed February 13, 2018).
[5] B. Regaard, S. Kaierle, R. Poprawe, Seam-tracking for high precision laser welding applications – methods, restrictions and enhanced concepts, J. Laser Appl. 21 (2010) 183–195.
[6] H. Chen, K. Liu, G. Xing, Y. Dong, H. Sun, W. Lin, A robust visual servo control system for narrow seam double head welding robot, Int. J. Adv. Manuf. Technol. 71 (2014) 1849–1860, https://doi.org/10.1007/s00170-013-5593-6.
[7] S. Krämer, W. Fiedler, A. Drenker, P. Abels, Seam tracking with texture based image processing for laser materials processing. vol. 8963, 2014, pp. 89630P–89630P–9, http://doi.org/10.1117/12.2040483.
[8] Y. Huang, Y. Xiao, P. Wang, M. Li, A seam-tracking laser welding platform with 3D and 2D visual information fusion vision sensor system, Int. J. Adv. Manuf. Technol. (2012) 415–426, https://doi.org/10.1007/s00170-012-4494-4.
[9] X. Gao, D. You, S. Katayama, Infrared image recognition for seam tracking monitoring during fiber laser welding, Mechatronics (2012) 370–380, https://doi.org/10.1016/j.mechatronics.2011.09.005.
[10] X. Gao, L. Mo, D. You, Z. Li, Tight butt joint weld detection based on optical flow and particle filtering of magneto-optical imaging, Mech. Syst. Signal Process. (2017) 16–30, https://doi.org/10.1016/j.ymssp.2017.04.001.
[11] Prometec, Prometec. http://www.prometec.com/ (accessed February 13, 2018).
[12] R. Olsson, I. Eriksson, J. Powell, A.V. Langtry, A.F.H. Kaplan, Challenges to the interpretation of the electromagnetic feedback from laser welding, Opt. Lasers Eng. (2011) 188–194, https://doi.org/10.1016/j.optlaseng.2010.08.018.
[13] I. Eriksson, A.F. Kaplan, Evaluation of laser weld monitoring – a case study, Proceedings of ICALEO (2009) 1419–1425.
[14] I. Eriksson, J. Powell, A.F.H. Kaplan, Signal overlap in the monitoring of laser welding, Meas. Sci. Technol. (2010) 105705, https://doi.org/10.1088/0957-0233/21/10/105705.
[15] A.F. Kaplan, P. Norman, I. Eriksson, Analysis of the keyhole and weld pool dynamics by imaging evaluation and photodiode monitoring, in: Proceedings of LAMP 2009 – 5th Int. Congr. Laser Adv. Mater. Process., 2009, pp. 1–6.
[16] Y. Kawahito, T. Ohnishi, S. Katayama, In-process monitoring and feedback control for stable production of full-penetration weld in continuous wave fibre laser welding, J. Phys Appl. Phys. (2009) 085501, https://doi.org/10.1088/0022-3727/42/8/085501.
[17] C. Bagger, F.O. Olsen, Laser welding closed-loop power control, J. Laser Appl. 19–24 (2003).
[18] S.-H. Baik, M.-S. Kim, S.-K. Park, C.-M. Chung, C.-J. Kim, K.-J. Kim, Process monitoring of laser welding using chromatic filtering of thermal radiation, Meas. Sci. Technol. (2000) 1772, https://doi.org/10.1088/0957-0233/11/12/317.
[19] P. Norman, H. Engström, A.F.H. Kaplan, Modelling of the impact of melt surface dynamics on a photodiode, monitoring signal in laser welding, Proceedings of ICALEO, (2007).
[20] Y.W. Park, H. Park, S. Rhee, M. Kang, Real time estimation of CO_2 laser weld quality for automotive industry, Opt. Laser Technol. 34 (2002) 135–142, https://doi.org/10.1016/S0030-3992(01)00103-7.
[21] S.S. Rodil, R.A. Gómez, J.M. Bernárdez, F. Rodríguez, L.J. Miguel, J.R. Perán, Laser welding defects detection in automotive industry based on radiation and spectroscopical measurements, Int. J. Adv. Manuf. Technol. (2010) 133–145, https://doi.org/10.1007/s00170-009-2395-y.
[22] C. Chui, An Introduction to Wavelets, Academic Press, New York, NY, USA, 1992.
[23] R.M. Rao, A.S. Bopardikar, Wavelet Transforms: Introduction to Theory & Applications, Longman Pub Group, Reading, MA, 1998.
[24] H. Luo, H. Zeng, L. Hu, X. Hu, Z. Zhou, Application of artificial neural network in laser welding defect diagnosis, J. Mater. Process. Technol. (2005) 403–411, https://doi.org/10.1016/j.jmatprotec.2005.06.008.

[25] H. Zeng, Z. Zhou, Y. Chen, H. Luo, L. Hu, Wavelet analysis of acoustic emission signals and quality control in laser welding, J. Laser Appl. (2001) 167–173, https://doi.org/10.2351/1.1386799.
[26] C. Steiger, T. Grünberger, A. Braunsteiner, M. Bohrer, M. Bammer, Application of wavelets for online laser process observer, Wavelet Applications VIII, in: Harald H. Szu, David L. Donoho, W. Adolf, William J. Lohmann, James R. Campell, Buss, (Eds.), Proceedings of SPIE, 4391 2001.
[27] N. Wu, J. Xiao, S. Chen, Wavelet Analysis based Splashing Identification in Electrode Pressure Sensing of Servo-torch Resistance Spot Welding, IIW-Doc III-1808-17.
[28] T. Sibillano, A. Ancona, D. Rizzi, V. Lupo, L. Tricarico, P.M. Lugarà, Plasma plume oscillations monitoring during laser welding of stainless steel by discrete wavelet transform application, Sensors (2010) 3549–3561, https://doi.org/10.3390/s100403549.
[29] D. You, X. Gao, S. Katayama, WPD-PCA based laser welding process monitoring and defects diagnosis by using FNN and SVM, IEEE Trans. Ind. Electron. (2014), https://doi.org/10.1109/TIE.2014.2319216.
[30] F. Vakili-Farahani, J. Lungershausen, K. Wasmer, Wavelet analysis of light emission signals in laser beam welding, J. Laser Appl. (2017) 022424, https://doi.org/10.2351/1.4983507.
[31] M. Farge, Wavelet transforms and their applications to turbulence, Annu. Rev. Fluid Mech. (1992) 395–458, https://doi.org/10.1146/annurev.fl.24.010192.002143.
[32] C. Torrence, G.P. Compo, A practical guide to wavelet analysis, Bull. Am. Meteorol. Soc. 61–78 (1998).
[33] S. Orfanidis, Introduction to Signal Processing, US Ed ed., Prentice Hall, Englewood Cliffs, N.J, 1995.
[34] M. Nilsen, F. Sikström, A.-K. Christiansson, A. Ancona, Vision and spectroscopic sensing for joint tracing in narrow gap laser butt welding, Opt. Laser Technol. (2017) 107–116, https://doi.org/10.1016/j.optlastec.2017.05.011.